A Theoretical Analysis of the Sum Frequency Generation Spectrum of the Water Surface. II. Time-Dependent Approach

Akihiro Morita

Department of Chemistry, Graduate School of Science, Kyoto University, Kyoto 606-8502, Japan

James T. Hynes*

Department of Chemistry and Biochemistry, University of Colorado, Boulder, Colorado 80309-0215, and Département de Chimie, CNRS UMR 8640, PASTEUR, Ecole Normale Supérieure, 24 rue Lhomond, Paris 75231, France

Sum frequency generation (SFG) spectroscopy is a powerful experimental technique to probe surface structures. This paper presents a new theoretical mode of nonempirical analysis of SFG spectra for interfacial structures, which considerably generalizes our previous effort (*Chem. Phys.* **2000,** *258,* 371), which involved several empirical elements. The method is based on a time correlation function for the frequency-dependent hyperpolarizability, which can be straightforwardly evaluated via molecular dynamics simulations and which explicitly takes into account, for example, intramolecular vibrations and electronic polarization. The new theory is capable of precisely describing a number of factors significant for the spectrum, such as the dielectric local field correction, vibrational dephasing, inter/intramolecular vibrational coupling, etc., and is fairly nonempirical and rigorous, within the dipole approximation. The results for the water−vapor interface reproduce the experimental spectra fairly well, although with some discrepancies; possible reasons for these are suggested.

1. Introduction

Sum frequency generation (SFG) and second harmonic generation (SHG) spectroscopies are powerful experimental techniques capable of probing interfacial structures.[1−6] These nonlinear spectroscopies owe their interfacial sensitivity to the breakdown of inversion symmetry at interfaces, within the dipolar approximation, in contrast to most of the other surface-sensitive techniques and therefore do not require ultrahigh vacuum conditions. This feature renders these techniques applicable for a wide range of investigations associated with liquid (solid)−gas surfaces in ambient conditions or even liquid (solid)−liquid interfaces. In the field of atmospheric chemistry, for example, both SFG and SHG have been applied to explore surfaces relevant to atmospheric aerosols,[7−12] and these spectroscopies are especially promising as a route to provide detailed surface structures under (comparatively) high atmospheric pressure conditions. Of special interest is the feature that SFG is a surface vibrational spectroscopy. In particular, SFG is, in principle, able to give the vibrational structures at interfaces as a combination of two input fields, fixed visible and tunable infrared (IR) in frequency.

To fully realize the potential usefulness of SFG, theoretical analysis will often be indispensable to interpret observed spectra in terms of microscopic surface structures. As just one illustration of the urgent need for such theoretical analyses, we cite the conflicting interpretations for the SFG spectra of sulfuric acid/water solutions,[13,14] a laboratory model for sulfate aerosols in the atmosphere.

While the basic overall formal theoretical framework of SFG spectroscopy has long been established,[15,16] a molecular-level theoretical interpretation of SFG spectra is still far from complete. One main difficulty arises from a lack of molecular information concerning the various parameters that are involved in and form essential ingredients of the formal theory, particularly frequency-dependent molecular hyperpolarizabilities and perturbations of them in condensed phase environments. Accordingly, relatively few attempts have been made to actually interpret the experimental spectra in detailed terms,[17−19] largely via empirical assumptions concerning those unknown parameters.

Recently, we presented the first attempt to simulate and analyze nonempirically the SFG spectrum of water surface with considerable success.[20] Our treatment included a modeling of the frequency-dependent hyperpolarizability via quantum chemical calculations and sampling of the surface structures via molecular dynamics (MD) simulations. An essentially similar method was subsequently employed by Yeh et al.[21] for the acetone surface.

Despite the encouraging success of our previous theoretical description, we noted[20] the need to generalize our treatment, especially in connection with further applications. One limitation inherent in our original treatment is that it is not completely nonempirical but was somewhat "optimized" for the water surface. In particular, several ingredients were derived neither from quantum chemical calculations nor from simulations, that is, the values of the nonresonant component of the frequency-dependent nonlinear susceptibility and that of the damping constant in the perturbation expression of the resonant component. These parameters affect the simulated spectra substantially—especially the nonresonant component—and thus their empirical estimation could restrict the predictive ability of our theoretical treatment for other systems. Another limiting aspect is that our treatment circumvented the explicit treatment of molecular vibrations via certain fitting procedures; although the associated

approximations were justified in detail for the water system, it is not clear whether such a treatment will always be valid, or even convenient, for other systems, particularly those involving complex, multicomponent surfaces. Because one of our ultimate principal goals is to theoretically predict and analyze complex surfaces of atmospheric relevance and reactions on them,[22] the removal of this limitation is of special importance.

Accordingly, the present paper presents a refined treatment of the simulation and analysis of SFG spectra. The new theory is based on a time-dependent formulation of the hyperpolarizability[23] via a flexible molecular model. This new version eliminates most of the above-mentioned restrictions in the original treatment and thus gives a fully nonempirical method for the SFG simulation. Further, the MD simulation takes account of the effect of electronic polarization so that the dielectric local field correction for the hyperpolarizability is also naturally incorporated. We believe that the present treatment should be very accurate within the classical MD methodology, the current models of MD configurations, and the dipole approximation of the SFG theory. The first application of this new treatment is given for the SFG spectrum of the water surface.

The remainder of this paper is organized as follows. Sections 2 and 3 deal with the theoretical formulation of the time-dependent treatment and the electronic polarization effect, respectively. Section 4 describes the modeling of the dipole and polarizability of a water molecule via quantum chemical calculations, and section 5 outlines the procedure for the MD simulations of the water surface. The results are given and discussed in section 6. Brief concluding remarks follow in section 7.

2. Time-Dependent Formalism for the Hyperpolarizability

Because SFG spectra are essentially determined by the frequency-dependent hyperpolarizability in a molecular level description,[16] we begin with the microscopic expression of the frequency-dependent molecular hyperpolarizability $\beta_{pqr}(\omega_{SFG},\omega_{vis},\omega_{IR})$; this will then be connected to the SFG signal. As shown in Appendix A, β_{pqr} generally consists of the resonant and nonresonant terms,

$$\beta_{pqr}(\omega_{SFG},\omega_{vis},\omega_{IR}) = \beta_{pqr}^R + \beta_{pqr}^{NR} \tag{1}$$

where p, q, and r are space-fixed axes and the resonant term, β_{pqr}^R, is represented via the perturbation formula,[15]

$$\beta_{pqr}^R = \sum_{v,v'}^{\text{vib. state}} \frac{\langle v|\alpha_{pq}|v'\rangle\langle v'|\mu_r|v\rangle}{(\omega_{v'} - \omega_v) - \omega_{IR} - i\gamma_{v'v}}\rho_v \tag{2}$$

with the IR frequency, ω_{IR}, possibly resonant with the vibrational energy gap, $\omega_{v'} - \omega_v$. (We use atomic units throughout.) In eq 2, ρ_v is the thermal distribution function of the initial vibrational states, v. α_{pq} is the molecular polarizability, μ_r is the molecular dipole moment, and $\gamma_{v'v}$ is a damping factor. Equation 2 is slightly more general than the corresponding equation in our previous SFG paper,[20] because the summations over all vibrational states, v and v', are taken into account here. Equation 2 is reexpressed in time-dependent form using the simple relation

$$\int_0^\infty dt\, e^{-i((\omega_{v'} - \omega_v) - \omega_{IR} - i\gamma_{v'v})t} = \frac{-i}{(\omega_{v'} - \omega_v) - \omega_{IR} - i\gamma_{v'v}} \tag{3}$$

as follows:

$$\beta_{pqr}^R = i\int_0^\infty dt \sum_{v,v'} e^{-i((\omega_{v'} - \omega_v) - \omega_{IR} - i\gamma_{v'v})t} \langle v|\alpha_{pq}|v'\rangle\langle v'|\mu_r|v\rangle\rho_v$$

$$= i\int_0^\infty dt \sum_{v,v'} e^{i\omega_{IR}t} \langle v|e^{iHt}\alpha_{pq}\,e^{-iHt}|v'\rangle\langle v'|\mu_r|v\rangle\rho_v$$

$$= i\int_0^\infty dt\, e^{i\omega_{IR}t} \langle\alpha_{pq}(t)\mu_r(0)\rangle \tag{4}$$

where the Hamiltonian, H, refers to the dynamics with zero external field. Equation 4 represents the resonant term of the molecular hyperpolarizability in terms of the Fourier–Laplace transformation of the time correlation function $\langle\alpha_{pq}(t)\mu_r(0)\rangle$.[23,25] While eq 4 is formally equivalent to eq 2, eq 4 does not explicitly include the damping factor $\gamma_{v'v}$ in eq 2, because the dephasing is naturally incorporated in the time development of the off-diagonal matrix elements during the MD calculations.

As discussed in Appendix A, the nonresonant term, β_{pqr}^{NR}, in eq 1 is an assembly of the terms other than eq 2 in the third-order perturbation expression of β_{pqr}, formally off-resonant with the vibrational energy gap, $\omega_{v'} - \omega_v$. Because experiments usually employ visible and SFG frequencies far from resonant conditions, the nonresonant term β^{NR} can be considered totally off-resonant and thus insensitive to the light frequencies involved. Therefore, neglecting the frequency dependence of the nonresonant term, we evaluated it with the static hyperpolarizability, which is readily calculated by an ab initio molecular orbital (MO) suite,

$$\beta_{pqr}^{NR} = \sigma\beta_{pqr}^{\text{static}} \tag{5}$$

where $\sigma = {}^1/_2$ is a symmetry number among the indices p, q, and r, which is discussed in Appendix B.

The time correlation function (tcf) treatment has several practical advantages in the simulations to obviate various approximations and assumptions associated with our previous approach. In particular, this treatment involves an improved treatment for the following factors: (1) the nonresonant term, β^{NR}, and the damping factor, γ, in the hyperpolarizability, (2) the modeling of the frequency shifts, (3) the intra- and intermolecular vibrational couplings, and (4) the local field correction.

Item 1 has been discussed above in this section. The present MD simulations with explicit internal vibrations are capable of describing the frequency shift and the vibrational couplings as a consequence of the intra/intermolecular force fields and obviate the need to introduce extra modelings for items 2 and 3. The local field correction in item 4 is also naturally incorporated in the present treatment using a polarizable model, as discussed fully in section 3.

The frequency-dependent nonlinear susceptibility of the entire system, χ_{pqr}, is expressed in the same way as the molecular hyperpolarizability,

$$\chi_{pqr} = \chi_{pqr}^R + \chi_{pqr}^{NR} \tag{6}$$

$$\chi_{pqr}^R = i\int_0^\infty dt\, e^{i\omega_{IR}t}\langle A_{pq}(t)M_r(0)\rangle \tag{7}$$

$$\chi_{pqr}^{NR} = \langle \sum_i \sum_{q'r'}^{\text{molecule}\,x-z} \beta_{pq'r'}^{NR}(i)f_{q'q}(i)f_{r'r}(i)\rangle \tag{8}$$

where the indices p-r in eqs 6–8 denote space-fixed coordinates. $A_{pq}(t)$ is the polarizability of the entire system at time t, and $M_r(0)$ is the total polarization at time 0. $f(i)$ in eq 8 is the local field correction factor for the i-th molecule, which will be

Theoretical Analysis of SFG Spectrum

J. Phys. Chem. B, Vol. 106, No. 3, 2002 **675**

derived in section 3 (see eq 21). The effect of the local field correction in the resonant term, eq 7, has been implicitly incorporated in the total polarizability, A, and polarization, M, involving all of the intermolecular electrostatic couplings.

Our basic strategy is to directly evaluate via classical MD simulations χ^R and χ^{NR} in eqs 7 and 8, where A, M, and β^{NR} are expressed on the basis of quantum chemical calculations. The present tcf treatment can be regarded as a natural extension of the theory of IR or Raman spectra based on the autocorrelation functions of $\mu(t)$ or $\alpha(t)$.[24] While the present work appears to be the first full MD implementation of the tcf approach for SFG, closely related tcf's have been used in more limited contexts in connection with SFG. Recently, Pouthier et al. developed a theoretical model based on the tcf formula to analyze the band shapes of the surface IR and SFG of an ordered monolayer absorbed on a clean surface.[23] They expressed the tcf using a model Hamiltonian from spectral density and relaxation of phonon modes, which was evaluated via MD simulations, employing empirical polarizability, dipole moment, and force field expressions. Wei and Shen have discussed the effect of rotational motion on SFG spectra using a time correlation function;[25] our treatment of simulations incorporates general molecular motions including translation, vibration, and rotation.

The SFG line shape, $I^{SFG}(\omega_{SFG}, \omega_{vis}, \omega_{IR})$, is then expressed in terms of the nonlinear susceptibility, χ, via[5]

$$I^{SFG}_{pqr} \propto \left(\frac{\omega_{SFG}}{\omega_{IR}}\right)^2 |\chi_{pqr}|^2 \qquad (9)$$

where the absolute intensity depends on the experimental geometry. The experimental light polarization is represented by either s or p, where s is the polarization parallel to the surface and p is the polarization perpendicular to both s and the light direction. In the ssp combination, which most experiments have employed to date, the relevant χ component is χ_{XXZ}(or χ_{YYZ}), where Z is normal to the surface and X and Y are two axes parallel to the surface.[20]

3. Effects of Electronic Polarization

As mentioned in the Introduction, a merit of the present approach is the explicit treatment of the electronic polarization effects on the SFG spectra. Here, we discuss two aspects associated with the electronic polarization: the enhancement of transition moments (in hydrogen-bonded systems such as water) and the local field correction.

3.1. Transition Moment Enhancement. Electronic polarization is essential to incorporate the well-known feature that the transition dipole moment of, for example, an OH stretch vibration is greatly enhanced because of hydrogen-bond formation, experimentally evidenced by the marked enhancement of the IR intensity of hydrogen-bonded OH stretching vibrations.[26,27] This remarkable enhancement has been interpreted via induced electronic polarization and/or charge transfer occurring within the hydrogen bonds associated with the vibration;[28,29] in the present model, we employ only the induced electronic polarization.[30] The effect is certainly expected to be significant in the water SFG spectrum because the transition dipole moment $\langle v|\mu|v'\rangle$ is involved explicitly in eq 2 or implicitly in eq 4. We will examine the explicit impact of this in section 6.

3.2. Local Field Correction. The second aspect of the electronic polarization is the local field correction, a dielectric effect in condensed phase environments referring to the difference between the external electric field and the internal field that each molecule feels.[31] This local field correction can be well defined and evaluated in the polarizable treatment, the details of which are now described.

For a system consisting of N molecules with polarizability α_i and permanent dipole moment $\vec{p}_i^0$ under an external field $\vec{E}^0$, the complete polarization (permanent + induced) of the i-th molecule, $\vec{p}_i$, is given as

$$\vec{p}_i = \vec{p}_i^0 + \alpha_i \vec{E}_i = \vec{p}_i^0 + \alpha_i(\vec{E}^0 - \sum_{j(\neq i)}^{N} T(\vec{r}_{ij})\vec{p}_j) \qquad (10)$$

where $\vec{E}_i$ is the local field at the i-th molecule and $T(\vec{r}_{ij})$ is the dipole field tensor:

$$T(\vec{r}_{ij}) = T_{ij} = \frac{1}{r_{ij}^3} - \frac{3}{r_{ij}^5}\begin{bmatrix} x_{ij}^2 & x_{ij}y_{ij} & x_{ij}z_{ij} \\ y_{ij}x_{ij} & y_{ij}^2 & y_{ij}z_{ij} \\ z_{ij}x_{ij} & z_{ij}y_{ij} & z_{ij}^2 \end{bmatrix}$$

Equation 10 can be represented in the matrix notation of $3N$ dimensions,

$$\mathbf{p} = \mathbf{p}^0 + \alpha\mathbf{E} = \mathbf{p}^0 + \alpha(\mathbf{E}^0 - \mathbf{Tp}), \qquad (11)$$

where

$$\mathbf{p} = \begin{bmatrix} \vec{p}_1 \\ \vdots \\ \vec{p}_N \end{bmatrix}, \quad \mathbf{p}^0 = \begin{bmatrix} \vec{p}_1^0 \\ \vdots \\ \vec{p}_N^0 \end{bmatrix}, \quad \alpha = \begin{bmatrix} \alpha_1 & & \\ & \ddots & \\ & & \alpha_N \end{bmatrix}, \quad \mathbf{E} = \begin{bmatrix} \vec{E}_1 \\ \vdots \\ \vec{E}_N \end{bmatrix},$$

$$\mathbf{E}^0 = \begin{bmatrix} \vec{E}^0 \\ \vdots \\ \vec{E}^0 \end{bmatrix}, \quad \mathbf{T} = \begin{bmatrix} 0 & T_{12} & \cdots & & \cdots & T_{1N} \\ T_{21} & 0 & & & & T_{2N} \\ \vdots & & \ddots & & & \vdots \\ \vdots & & & & 0 & T_{N-1N} \\ T_{N1} & \cdots & & \cdots & T_{NN-1} & 0 \end{bmatrix}$$

so that the formal solutions of $\mathbf{E}$ and $\mathbf{p}$ are

$$\mathbf{E} = \mathbf{E}^0 - \mathbf{Tp} = (1 + \mathbf{T}\alpha)^{-1}(\mathbf{E}^0 - \mathbf{Tp}^0) \qquad (12)$$

$$\mathbf{p} = \mathbf{p}^0 + \alpha\mathbf{E} = (1 + \alpha\mathbf{T})^{-1}(\mathbf{p}^0 + \alpha\mathbf{E}^0) \qquad (13)$$

This then gives the effective polarizability, α^{eff}, defined as the derivative of the overall polarization, eq 13, with respect to the external field

$$\alpha^{eff} = \partial\mathbf{p}/\partial\mathbf{E}^0 = (1 + \alpha\mathbf{T})^{-1}\alpha = \alpha(1 + \mathbf{T}\alpha)^{-1} \qquad (14)$$

where α^{eff} is a $3N \times 3N$ matrix represented with component tensors α_{ij}^{eff} of 3×3 dimension as

$$\alpha^{eff} = \begin{bmatrix} \alpha_{11}^{eff} & \cdots & \alpha_{1N}^{eff} \\ \vdots & \ddots & \vdots \\ \alpha_{N1}^{eff} & \cdots & \alpha_{NN}^{eff} \end{bmatrix}$$

Each component, α_{ij}^{eff}, indicates the induced polarization of the i-th molecule when the j-th molecule is under the influence of the external field. Note that there are the nonzero matrix elements between different molecules ($\alpha_{ij}^{eff} \neq 0$ for $i \neq j$) owing to intermolecular electrostatic coupling. With the assumption that the external field is uniform in space—a good approximation for microscopic systems with typical light fields—

the polarizability, A, of the entire system is given as the simple sum of the component effective polarizabilities and the polarization, M, consists of the summed molecular dipole moments:

$$A = \sum_i^N \sum_j^N \alpha_{ij}^{\text{eff}}, \quad M = \sum_i^N \vec{p}_i \quad (15)$$

These are utilized to construct the time correlation function in eq 7.

The effective polarizability and the polarization are expressed using a local field correction tensor now introduced. The local field correction is defined as the derivative of the internal field $\mathbf{E}$ with respect to the external field $\mathbf{E}^0$. Therefore, eq 12 gives the local field correction tensor $\mathbf{g}$ of $3N \times 3N$ dimension as

$$\mathbf{g} = (1 + \mathbf{T}\alpha)^{-1} \quad \text{or} \quad \mathbf{g}^{\text{T}} = (1 + \alpha\mathbf{T})^{-1} \quad (16)$$

The second expression of eq 16 denotes the transposition of $\mathbf{g}$ because α and $\mathbf{T}$ are symmetric matrices. Equations 12, 13, and 14 are then reexpressed using the local field correlation tensor as follows:

$$\mathbf{E} = \mathbf{g} \cdot (\mathbf{E}^0 - \mathbf{T}\mathbf{p}^0) \quad (17)$$

$$\mathbf{p} = \mathbf{g}^{\text{T}} \cdot (\mathbf{p}^0 + \alpha\mathbf{E}^0) \quad (18)$$

$$\alpha^{\text{eff}} = \mathbf{g}^{\text{T}} \cdot \alpha = \alpha \cdot \mathbf{g} \quad (19)$$

Note that in the general case where α is not a scalar matrix, the corrections for the field $\mathbf{E}$ and for the polarization $\mathbf{p}$ are not necessarily identical.

The nonresonant component of the susceptibility, χ_{pqr}^{NR} in eq 8, is also affected by the local field correction because the two input external electric fields are modified in a dielectric via eq 17. Therefore, χ_{pqr}^{NR} is expressed as the sum of nonresonant hyperpolarizabilities of constituent molecules with the local field correction

$$\chi_{pqr}^{\text{NR}} = \left\langle \sum_{i,j,k}^N \sum_{q'r'}^{x-z} \beta_{pq'r'}^{\text{NR}}(i)[g_{ij}]_{q'q}[g_{ik}]_{r'r} \right\rangle$$

$$= \left\langle \sum_i^N \sum_{q'r'}^{x-z} \beta_{pq'r'}^{\text{NR}}(i) f_{q'q}(i) f_{r'r}(i) \right\rangle \quad (20)$$

which leads to eq 8. There, $f_{pq}(i)$ is the local field correction factor for the i-th molecule, defined as

$$f_{pq}(i) \equiv \sum_j^N [g_{ij}]_{pq} \quad (21)$$

In the actual calculations during MD simulations, explicit evaluation of $\mathbf{g}$ of eq 16 via matrix inversion would be quite time-consuming but is, in fact, not necessary. To calculate the time correlation function $\langle A(t)M(0)\rangle$ and the nonresonant susceptibility χ^{NR}, we need only A and M in eq 15 and f in eq 21. Therefore, at each time step of the MD simulations, the two equations,

$$(1 + \mathbf{T}\alpha)\mathbf{E} = \mathbf{E}^0 - \mathbf{T}\mathbf{p}^0 \quad (22)$$

$$(1 + \mathbf{T}\alpha)\mathbf{f} = \mathbf{h} \quad (23)$$

with the common coefficient matrix have to be solved for $\mathbf{E}$ and $\mathbf{f}$, where $\mathbf{f}$ and $\mathbf{h}$ in eq 23 are $3N \times 3$ matrices,

$$\mathbf{f} = \begin{bmatrix} f(1) \\ \vdots \\ f(N) \end{bmatrix}, \quad \mathbf{h} = \begin{bmatrix} 1 \\ \vdots \\ 1 \end{bmatrix}$$

The above component $f(i)$ is a 3×3 matrix of the local field correction factor for the i-th molecule, that is, $[f(i)]_{pq} = f_{pq}(i)$ in eq 21, and the component 1 denotes the 3×3 unit matrix. The solution for $\mathbf{E}$ in eq 22 defines the electric field in the polarizable environment, and it gives the overall polarization M via eqs 11 and 15 as

$$M = \sum_i^N \vec{p}_i = \sum_i^N (\vec{p}_i^0 + \alpha_i \vec{E}_i) \quad (24)$$

The solution for $\mathbf{f}$ gives the local field correction factor in eq 21, and the polarizability, A, of the entire system is thus represented as

$$A = \sum_i^N \sum_j^N \alpha_{ij}^{\text{eff}} = \sum_i^N \sum_j^N \alpha_i \cdot g_{ij} = \sum_i^N \alpha_i \cdot f(i) \quad (25)$$

using eqs 15, 19, and 21.

4. Water Molecule Modeling

Prior to the actual MD calculations of the time correlation function $\langle A(t)M(0)\rangle$ using the flexible molecular model, the dipole moment and the polarizability of a water molecule need to be represented in analytic forms as a function of the internal molecular geometry. These analytic forms have been determined via a fitting of quantum chemical calculations, now described.

The quantum chemical calculations were performed for a water molecule with varying geometry using the B3LYP density functional theory[32,33] implemented in Gaussian 98.[34] The basis sets employed are d-aug-cc-pVDZ for the oxygen atom and aug-cc-pVDZ for hydrogen atoms,[35] a level of accuracy sufficient to reproduce the experimental dipole moment and polarizability.[36] A total of 324 molecular geometries were sampled in the range of $R_1, R_2 = R^{\text{eq}} - 2\delta_R \approx R^{\text{eq}} + 5\delta_R$ and $\theta = \theta^{\text{eq}} - 4\delta_\theta \approx \theta^{\text{eq}} + 4\delta_\theta$, where R_1 and R_2 are two O–H bond lengths, and θ is the H–O–H angle. R^{eq} and θ^{eq} are the equilibrium values;[37] $R^{\text{eq}} = 0.9575$ Å, and $\theta^{\text{eq}} = 104.51°$. δ_R and δ_θ are the spacings for sampling; $\delta_R = 0.05$ Å and $\delta_\theta = 5°$. The dipole moments and polarizabilities calculated at the above 324 geometries[38] were utilized in the least-squares fitting.

The analytic form of the dipole moment is derived as follows. The three components of the calculated dipole moment uniquely determine the point charges at the three nuclei, q_0, q_1, and q_2, where q_0 locates the oxygen site and q_1 and q_2 locate the two hydrogen sites. (The neutrality condition constraint is imposed on the partial charges, while one nonplanar dipole component inevitably vanishes.) At the equilibrium geometry of an isolated water, the partial charges are determined to be $q_0^{\text{eq}} = -0.6570$ and $q_1^{\text{eq}} = q_2^{\text{eq}} = 0.3285$. The displacements of the partial charges from their equilibrium values, Δq_0, Δq_1, and Δq_2, are related to the displacements of the internal coordinates from their equilibrium values, ΔR_1, ΔR_2, and $\Delta\theta$. Taking account of the two equivalent hydrogens, it is convenient to introduce the

Theoretical Analysis of SFG Spectrum

J. Phys. Chem. B, Vol. 106, No. 3, 2002 **677**

TABLE 1: The Parameters in Eqs 27, 28, and 29 to Represent the Dipole Moment and Polarizability of a Water Molecule with Varying Geometry

dipole moment (au)		polarizability (au)	
C_1	0.1396	D_1	4.6077
C_2	−0.1196	D_2	4.8894
C_3	−0.0164	D_3	5.5062
C_4	−0.0288	D_4	1.6890
C_5	−0.0516	D_5	1.6102
C_6	0.0532	D_6	7.3812
C_7	−0.0699	D_7	3.4710
C_8	0.0169		
C_9	0.1142		

symmetry-adapted coordinates of the displacements, X_1, X_2, and X_3, as

$$X_1 = \Delta R_1 + \Delta R_2, \quad X_2 = \Delta R_1 - \Delta R_2, \quad X_3 = \Delta\theta \quad (26)$$

Then, the symmetry-adapted displacements of the partial charges, Δq_0 and $\Delta q_1 - \Delta q_2$, are expressed as

$$\Delta q_0 = C_1 X_1 + C_2 X_3 + C_3 X_1^2 + C_4 X_2^2 + C_5 X_3^2 + C_6 X_1 X_3 \quad (27)$$

$$\Delta q_1 - \Delta q_2 = C_7 X_2 + C_8 X_1 X_2 + C_9 X_2 X_3 \quad (28)$$

where $C_1 - C_9$ are nine parameters determined via the least-squares fitting. The neutrality condition automatically accounts for the other symmetrized charge displacement, $\Delta q_1 + \Delta q_2$.

The analytic form of the polarizability consists of two bond polarizabilities associated with the two O−H bonds. Each bond polarizability, α_1 or α_2, is represented as

$$\alpha_i = \begin{bmatrix} D_1 + D_4\Delta R_i & & \\ & D_2 + D_5\Delta R_i & \\ & & D_3 + D_6\Delta R_i + D_7\Delta R_i^2 \end{bmatrix} \quad (29)$$

where $i = 1$, 2. The tensor is defined in the local frame associated with the O−H bond, where the z axis is parallel to the O−H bond and the xz plane contains the molecular plane with the other hydrogen on the positive side of the x axis. The overall molecular polarizability α can be well represented as the sum of two bond polarizabilities,

$$\alpha = A_1^\dagger \alpha_1 A_1 + A_2^\dagger \alpha_2 A_2 \quad (30)$$

where A_1 and A_2 are the rotational matrices, which convert the local frames to the molecular frame. The parameters $D_1 - D_7$ are also determined via the least-squares fitting.

The results for the fitting parameters are summarized in Table 1, and their fitting performance is shown in Figure 1. The overall accuracy is quite satisfactory, particularly in Figure 1a. In Figure 1b, some systematic deviations from the regression line are observed in (i) the large displacement region ($\sim$6 au) and (ii) the upper left side of the line in the small displacement region ($\sim$0 au). The former points are associated with geometries having both quite extended O−H distances and large H−O−H angles and hence are not energetically significant. The latter points are associated with a small off-diagonal component of the polarizability in the molecular frame diagonalizing the inertia
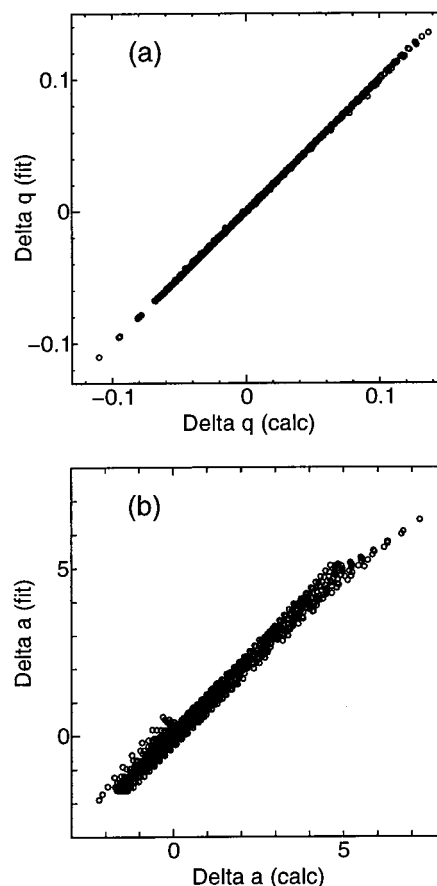

Figure 1. Fitting accuracy of (a) dipole moment and (b) polarizability of a water molecule. The fitted values (ordinates) are compared to the quantum chemical values (abscissas) at a total of 324 geometries. Panel a shows the displacements in the partial charges on the three atomic sites. Panel b shows the displacements in the four nonzero components (3 diagonal and 1 off-diagonal) of the polarizability tensor defined in the molecular frame diagonalizing the inertia tensor. Values are in units of au.

tensor. This off-diagonal in-plane component is far less important than the three main diagonal components by an order of magnitude. Consequently, we believe that further improvement in the fitting is unnecessary for implementation in the MD calculations.

5. Force Fields and MD Procedures

We have employed the flexible force field model of water developed by Ferguson.[39] This model is a revised version of the SPC model[40] to incorporate the intramolecular vibrations, involving parameter determination via the experimental neutron scattering density of states for the hydrogens,[41] and the Lennard-Jones parameters and the partial charges were accordingly reparametrized. We have also employed, for comparison, the different internal force field model due to Kuchitsu and Morino,[42] using the same Lennard-Jones parameters and partial charges. Both force fields are anharmonic; the Kuchitsu−Morino force field is accurate for a single isolated water molecule, while the Ferguson force field has been optimized particularly for condensed phase simulations.

The entire MD simulation system is an infinite thin film, attained via two-dimensional periodic boundary conditions, of which the thickness is about 25 Å (see Figure 2). The length of each periodic cell is 24.859 Å, and each periodic image contains 512 molecules. The MD simulations were performed with the
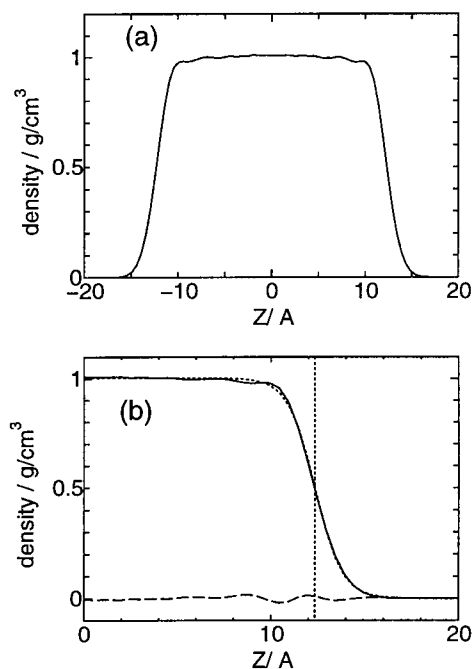
Figure 2. Calculated density profile of water (panel a). The Z axis of the abscissa is along the surface normal, where $Z = 0$ indicates the center of the film. Panel b compares the calculated density (solid line) with the fitted one by eq 32 (dotted line), where the horizontal dashed line is the difference between fitted and calculated values and the vertical dotted line is the Gibbs dividing surface at $Z = 12.3$ Å. Units are Å for the abscissas and g/cm^3 for the ordinates.

force fields described above, while the effects of electronic polarizability were taken into account in the trajectories thus generated.[43] The constant energy (microcanonical) time development was carried out by the velocity Verlet algorithm[44] with a time step of 0.6 fs. During the MD simulations, the intermolecular interactions were cut off at half of the periodic length with a tapering function and no long range correction was adopted.[45] The attenuating factor, $g(r)$, for the intermolecular potentials is given as

$$g(r) = \begin{cases} 1 & (r < 0.9r_c) \\ 1 - 10x^3 + 15x^4 - 6x^5 & (0.9r_c < r < r_c) \\ 0 & (r_c < r) \end{cases} \quad (31)$$

where $x = (r - 0.9r_c)/(0.1r_c)$ and r_c is the cutoff length. Here, r denotes the center-of-mass distance (and not the site−site distance).

The initial equilibration prior to the sampling run consists of two stages. In the first stage, it is the bulk configuration, which is mainly relaxed, while in the second stage it is the surface configuration. In the first stage, the equilibration was carried out for 6 ps employing three-dimensional periodic boundary conditions. The periodic lengths were 24.859 Å each, imposing the fixed density of 0.997 g/cm^3. The starting configurations for this stage were the fcc lattice of water locations with random molecular orientations. After this equilibration, one periodic boundary condition along the surface normal was removed, and further equilibration was carried out with two-dimensional periodic boundary conditions for 6 ps. Occasional temperature scaling was performed to maintain the system temperature at about 300 K during the equilibration stages.

The configurations thus prepared were used for the initial configurations to sample the surface structures and to calculate

the time correlation functions during 15 ps for each trajectory with no temperature control applied. A total of 640 trajectories with different initial configurations were generated, and the statistical averages were taken. The system temperature evaluated from the instantaneous kinetic energy was 301.7 ± 5.9 K.

In the calculations of the total dipole, M, and polarizability, A, at each time step, some attention has to be paid to the feature that the thin film has two sides of the surface having opposite surface normal vectors so that straightforward summation would lead to cancellation of the normal components. Therefore, at each time step, the entire system was divided at the center of the film ($Z = 0$), and the summations of eqs 24 and 25 were taken in the $Z > 0$ and $Z < 0$ regions separately. The quantities in the two regions are treated separately in the statistical averaging of the time correlation functions.

The MD calculations were performed on the Fujitsu VPP800 and VPP5000 vector parallel machines at the Kyoto University Data Processing Center in Kyoto and the Research Center of Computational Science in Okazaki. During the MD simulations, the calculations of the local field correction are most time-consuming. Those calculations, including solutions of the large linear equations eqs 22 and 23, were, however, considerably accelerated (by about a factor of 20) on the vector processors.

We have also simulated the spectra without the local field correction, using the force fields of Ferguson and of Kuchitsu and Morino to examine the effects of the local field correction and the different force fields. These calculations were performed on the IBM SP2 parallel computers at the Pacific Northwest National Laboratory.

6. Results and Discussion

6.1. Density Profile. The calculated vertical density profile with the Ferguson force field is shown in Figure 2a, where $Z = 0$ indicates the center of mass of the entire system. The density profile obtained with the Kuchitsu and Morino force fields for the internal flexibility is essentially the same. This reflects the feature that the density profile is not sensitive to the (different) internal force fields but is essentially determined by the intermolecular force field, which is the same in the two cases. This density distribution is well represented by[48,49]

$$\rho(Z) = a[1 - \tanh\{b(|Z| - c)\}] \quad (32)$$

where $a = 0.50$ g/cm^3, $b = 0.69$ Å^{-1}, and $c = 12.3$ Å so that the bulk density is $2a = 1.0$ g/cm^3 and the transition thickness at the surface measured from 10% to 90% of the bulk density is $2.1972/b = 3.18$ Å. The Gibbs dividing surfaces are located on either side of the film from the center of mass by $c = 12.3$ Å. The present 10%−90% thickness is slightly smaller than the result, 3.88 Å, of a previous simulation with the SPC/E water model,[50] indicating somewhat a more compact surface with the Ferguson water model.[51] Another noticeable density profile feature is a slight corrugation near the surface (see the dashed line of Figure 2b). This oscillation, implying a molecular-level structuring near the surface, is emphasized via the compact surface in the present water model.

6.2. Bulk Infrared Spectrum. It is useful for purposes of perspective to first briefly consider the usual IR spectrum of the OH stretching vibrations for the bulk region. The IR absorption cross section, $\sigma(\omega)$, is[24]

$$\sigma(\omega) = \frac{4\pi^2\omega(1 - e^{-\beta\hbar\omega})}{3\hbar c n(\omega)} I^{IR}(\omega) \quad (33)$$

Theoretical Analysis of SFG Spectrum
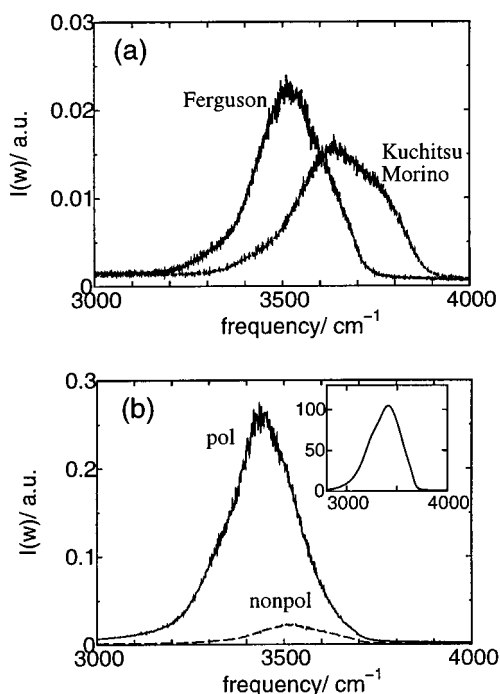
J. Phys. Chem. B, Vol. 106, No. 3, 2002 **679**

Figure 3. Calculated IR absorption line shapes, $I^{IR}(\omega)$, of the whole system. In panel a, the two force fields, Ferguson and Kuchitsu−Morino, are compared with no electronic polarization considered. In panel b, the spectrum with induced electronic polarization (denoted "pol") is compared to that without the electronic polarization ("nonpol") using the Ferguson force field. The latter line labeled "nonpol" is identical to the left line of panel a. The upper left corner of panel b shows the experimental IR absorption spectrum of water.[54] Reproduced with permission from ref 54. Copyright 1996, Society of Applied Spectroscopy. Values are in units of au; note that the polarization in the 2-dimensional unit cell is normalized by area and not by the volume. For the experimental IR spectrum, the unit is L/(mol cm).

where $n(\omega)$ is the refractive index of water as a function of frequency[52] and $I^{IR}(\omega)$ is the absorption line shape function,

$$I^{IR}(\omega) = \frac{1}{2\pi}\int_{-\infty}^{\infty} dt\, e^{-i\omega t}\langle M(0)\cdot M(t)\rangle \qquad (34)$$

$I^{IR}(\omega)$ essentially determines the line shape of the IR spectrum because the prefactor of eq 33 does not vary significantly in the OH stretching frequency region.[52] We have used the classical expression of eq 34 because the quantum correction does not alter the band shape in the limited frequency region considered here, 3000−4000 cm^{-1}.

As shown in Figure 3, the experimental IR spectrum of water in the OH stretching region consists of a single broad band with no significant structure at the peak located at about 3410−3450 cm^{-1}.[53,54] In the following, we analyze the effects of the internal force fields (Figure 3a) and of the induced polarization (Figure 3b) on this spectrum. Figure 3a exhibits the two absorption line shapes calculated with the Ferguson (F) and the Kuchitsu and Morino (KM) force fields. Both force fields reproduce an experimentally observed structureless feature of the IR spectrum. However, the peak positions for the F and KM models are located at ∼3500 and 3650 cm^{-1}, respectively, both blue-shifted from the experimental maximum at 3410−3450 cm^{-1}. The large frequency overestimation of KM is arguably due to the feature that the classical MD calculations do not properly sample the anharmonic potential energy region of the OH bonds; on the other hand, the F potential has been designed to be applicable

for classical simulations. We also notice a mild asymmetry with a longer tail in the lower-frequency region in the experimental IR spectrum of Figure 3. The asymmetry is slightly underestimated with the F model and overestimated with the KM model.

Figure 3b demonstrates the important twofold effect of the induced electronic polarization on the IR spectrum. First, the electronic polarization greatly enhances the IR intensity, by an order of magnitude.[26,27] Second, because the enhancement of the dipole transition moment is larger in the lower-frequency region because of strong hydrogen bonds,[20] the electronic polarization effect shifts the spectrum to the red by ∼100 cm^{-1} in the F model so that the peak position is located around 3430 cm^{-1}, in very good agreement with experiment. We note that the spectra with and without the electronic polarization were generated from the same trajectories of the MD simulation so that the vibrational density of states in the two spectra is identical. Therefore, the spectral shift is a consequence of the larger enhancement of the intensity in the lower-frequency region and not of any change in the vibrational density of states. Finally, the quite good agreement between experiment and the theory using the Ferguson model and including electronic polarization provides basic support for the present approach.

6.3. Surface IR. In the first simulation attempt to analyze surface vibrational spectroscopy, Benjamin calculated, as a simple alternative to SFG spectra, a hypothetical IR spectrum of the water surface, in which the polarization, M, in eq 34 was restricted to a certain surface region.[55] (A nonpolarizable water model was used.) While some resemblances were observed between this surface IR spectrum and experimental SFG spectra, it is not clear to what extent the analogy holds; accordingly, we briefly discuss the surface IR spectrum here.

Because the definition of the surface region is not unique, Figure 4a displays the calculated surface IR with different thresholds, Z_{thrs}, used to define the surface boundary, where the region $|Z| > Z_{thrs}$ is regarded as the surface ($Z_{thrs} = 10-14$ Å, see Figure 2). In these calculations, the Ferguson force field was employed. The calculated surface IR spectra exhibit two bands in the OH stretching frequency range, one at ∼3500 cm^{-1} and the other at ∼3700 cm^{-1}. This band shape is qualitatively different from the single broad band shape of the usual bulk IR spectrum in Figure 3 but is somewhat similar to that of the water SFG spectrum, which also has a two band structure (cf. section 6.4). The lower-frequency band is correlated to the main band of the bulk IR, while the higher-frequency band is evidently characteristic of the surface (and is overwhelmed in the usual bulk IR spectrum).

However, even if the surface IR very qualitatively reproduces the two-band structure of an SFG spectrum, the relative intensity of these two bands presents a serious difficulty because (a) it depends on the definition of the surface boundary and (b) it depends sensitively on the effect of the electronic polarization; as will now be seen, these two aspects combine to preclude a useful definition connecting the surface IR spectrum with the SFG spectrum. With regard to the surface definition, Figure 4a shows that the increase of the intensity of the lower-frequency band compared to that of the higher-frequency band increases as Z_{thrs} decreases, and eventually the lower band overwhelms the higher, as in the usual bulk IR. Even if we were to determine an optimized boundary to make the surface IR spectrum consistent with the SFG spectrum, this route is thwarted by the
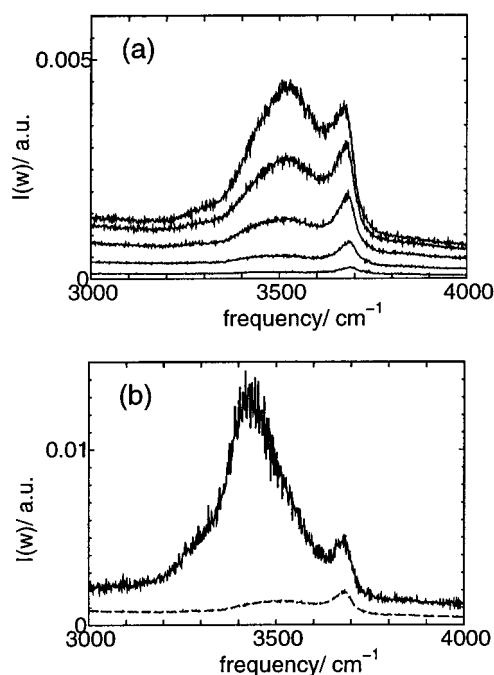
Figure 4. IR absorption line shapes, $I^{IR}(\omega)$, of the surface, where the polarization M in eq 34 is restricted to the surface region, $|Z| > Z_{thrs}$. In panel a, $Z_{thrs} = 10, 11, 12, 13,$ and 14 Å from the top to the bottom with no electronic polarization considered. Panel b compares $I^{IR}(\omega)$ with $Z_{thrs} = 12$ Å involving induced electronic polarization (solid line) to that with no electronic polarization (dashed line).

influence of the electronic polarization. For, as shown in Figure 4b, the relative intensity dramatically changes in the polarizable case so that the higher-frequency band at 3700 cm^{-1} becomes a small shoulder peak, which is then not consistent with the SFG band shape. (Recall from section 6.2 that the lower-frequency region gains larger enhancement in the intensity because of the electronic polarization.) Indeed, when the induced

polarization is included, we could not select a Z for which the surface IR spectrum peaks have the same intensity ratio as do the SFG spectrum ones. Thus, while the surface IR approach can be qualitatively useful, the direct simulation of the SFG spectrum would clearly be preferable.

6.4. Frequency-Dependent Nonlinear Susceptibility and SFG Spectrum. To begin the discussion of the SFG spectrum itself, we display in Figure 5 three previously reported experimental SFG spectra of liquid water with the *ssp* polarization. Although the three spectra from different groups have general similarities, they also show significant variation. The line shapes generally consist of a sharp band at ~3700 cm^{-1} and a broad one below ~3600 cm^{-1}. The high-frequency band, which exhibits little red shift from the OH stretching frequencies of an isolated water molecule, has been assigned as the OH stretching of the dangling hydrogen bonds at the surface, while the lower-frequency band with a large red shift has been attributed to hydrogen-bonded OH stretching vibrations.[9,56,57] However, considerable discrepancies are observed among the experimental spectra, particularly in the intensity ratio of the two bands and the line shape of the lower-frequency band. Panel c has distinctively small intensity of the higher-frequency band. The authors elucidated this as related to laser pulse temporal dephasing of their femtosecond laser system,[9] whereas other results with the use of a nanosecond laser do not suffer from the effect. Accordingly, we focus our attention only on the first two experimental SFG line shapes. The line shapes of the lower-frequency band also show considerable differences among the spectra, probably because of the different experimental setups and normalizing procedures,[9] although the source of the differences is not very clear.[58]

The calculated SFG line shapes of the *ssp* signal, I^{SFG}_{ssp} given by eq 9, are displayed in Figure 6, which involves three cases (panels a–c) corresponding to different force fields and treatments of the electronic polarization. In each case, the general feature of the two band structure is well reproduced. As we
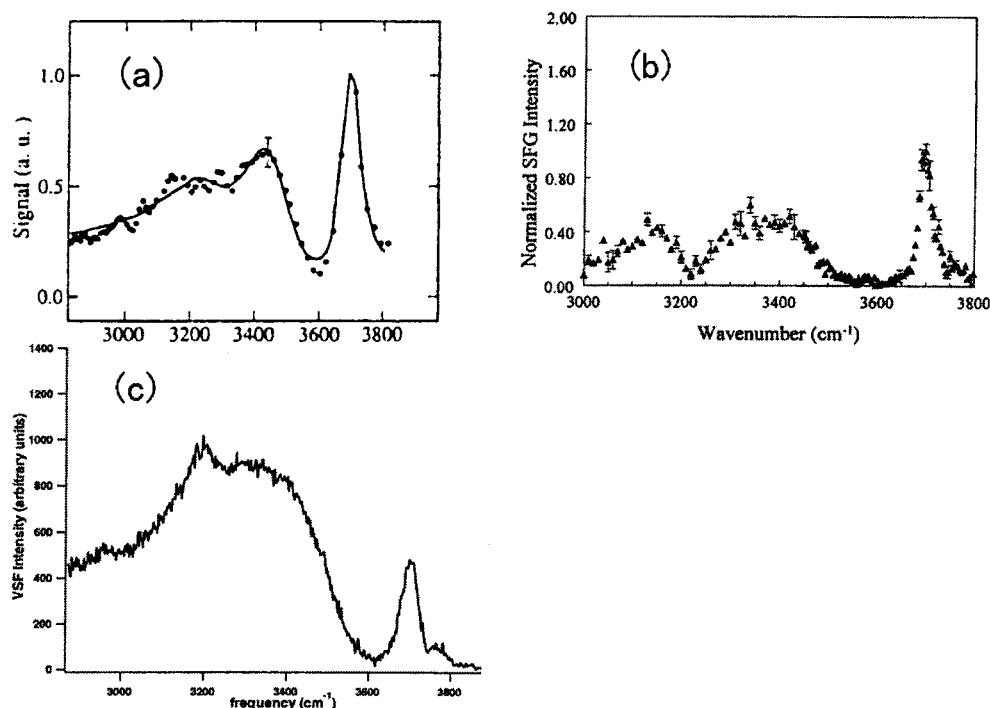

Figure 5. Experimental SFG spectra of liquid water of the *ssp* polarization. Panel a was reprinted with permission from ref 56. Copyright 1993, American Physical Society. Panel b was reprinted with permission from ref 57. Copyright 1999, American Chemical Society. Panel c was reprinted with permission from ref 9. Copyright 2001, American Chemical Society.
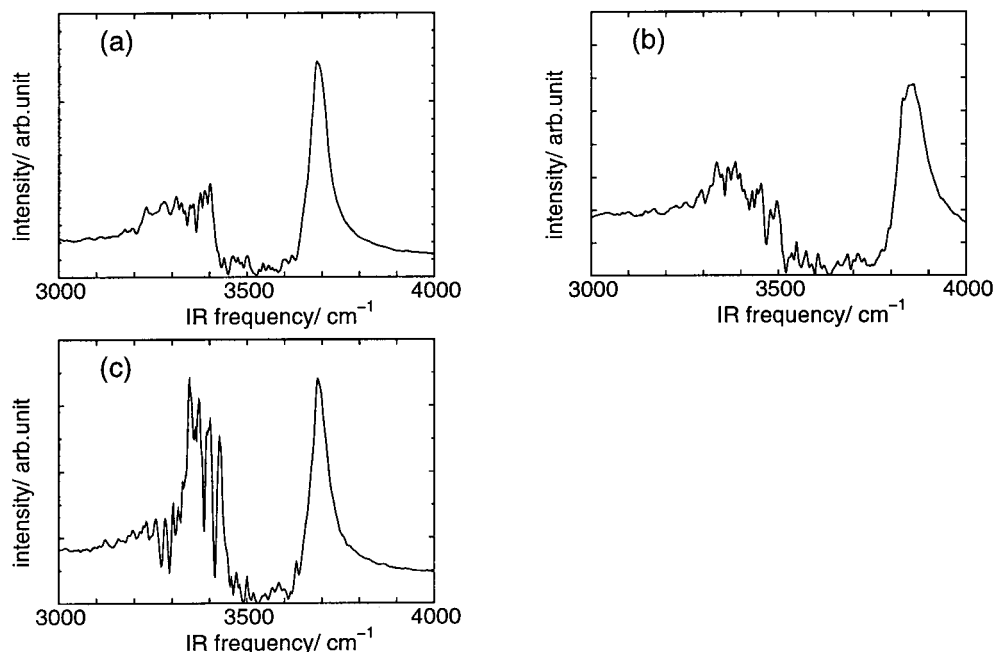
Theoretical Analysis of SFG Spectrum

J. Phys. Chem. B, Vol. 106, No. 3, 2002 **681**

Figure 6. Calculated *ssp* SFG spectrum of the water surface. Three models are employed: (a) the Ferguson force field with no induced polarization, (b) the Kuchitsu and Morino force field with no induced polarization, and (c) the Ferguson force field with induced electronic polarization. The abscissas indicate the tunable IR frequency in cm^{-1}, while the visible wavelength is fixed to be 532 nm. The intensity unit of the ordinates is arbitrary.

have discussed in detail in ref 20, the high-frequency band arises from the surface top monolayer, while the lower-frequency band has contributions from a few top monolayers of the surface. Comparing the two cases a and b, the KM force field result gives a high-frequency band considerably blue-shifted compared to experiment, as is to be expected from our discussion in section 6.2, and related to the sampling problem of the KM model in the anharmonic potential region. Concerning the relative intensity of the two bands, cases a and b with no electronic polarization included exhibit a small intensity for the lower-frequency band, while panel c shows that the induced electronic polarization enhances its intensity to be comparable to that of the higher-frequency peak. This is a consequence of the enhanced transition moment as discussed in section 6.2. Both panels a and c, involving the Ferguson force field, well reproduce the experimental location of the high-frequency band at around 3700 cm^{-1} (compare Figure 5). Panel c should be regarded as the most sophisticated theoretical result, including as it does the Ferguson force field and the electronic polarization (and concerning the latter, it is useful for perspective to recall the importance of this polarization for the bulk IR spectrum, cf. Figure 3b). Panel c gives the integrated intensity ratio between the lower- and higher-frequency bands closer to the experiments (Figure 5a,b), though the line shapes of the lower band certainly show significant disagreement between the calculation and the experimental results in Figure 5a,b (which do not agree with each other). We will comment in section 7 on an additional feature that may be necessary to examine in future work on the low-frequency band.

Some further detail can be provided in Figure 7, which displays the *XXZ* component of the nonlinear susceptibility of the water surface calculated via eqs 7 and 8, which is the component relevant for the SFG *ssp* spectrum. The three results (panels a−c) presented in Figure 7 all have the same qualitative shapes for the real and imaginary parts of χ, and they are also similar to our previous results.[20] The imaginary part changes

its sign at 3500−3600 cm^{-1}, implying different orientations of the surface water molecules of the two bands.[20] The arrows in Figure 7 indicate the nonresonant component, χ_{XXZ}^{NR}, calculated via eq 8 in the MD simulations. (Note that in the case without induced electronic polarization, the local field correction factor $f_{pq}(i) = \delta_{pq}$, and hence, eq 8 is replaced with $\chi_{pqr}^{NR} = \sum_i \beta_{pqr}^{NR}(i)$.) While the qualitative characteristics of the line shapes are not strongly sensitive to the models we have employed, the effects of the force fields and the induced electronic polarization discussed for the SFG spectrum itself are also observed in cases a−c of Figure 7: the frequency shift in comparison with panels a and b and the enhanced amplitude of the nonlinear susceptibility in the lower-frequency band region in panels a and c, respectively.

Altogether, these results generally indicate that the shape of the lower-frequency band is described with more difficulty than that of the higher-frequency one. This general feature is consistent with our remarks above and in ref 20 concerning the molecular origins of the bands. In particular, while the high-frequency band is essentially determined by the dangling OH bonds at the surface top monolayer, the lower band, arising from hydrogen-bonded OH stretching vibrations, is influenced by various factors in the surface region deeper than the top monolayer. We note again that the shape of the lower-frequency band seems to be difficult to reproduce even experimentally, as shown in the considerable variation of the band shapes in Figure 5.

7. Concluding Remarks

In this paper, we have developed a theoretical method to simulate SFG spectra as rigorously as possible, to fully exploit its potential usefulness as a probe of microscopic surface structure. We have employed a time-dependent formula for the hyperpolarizability and nonlinear susceptibility, which is suitable for straightforward evaluation of the susceptibility via molecular dynamics simulations, taking explicit account
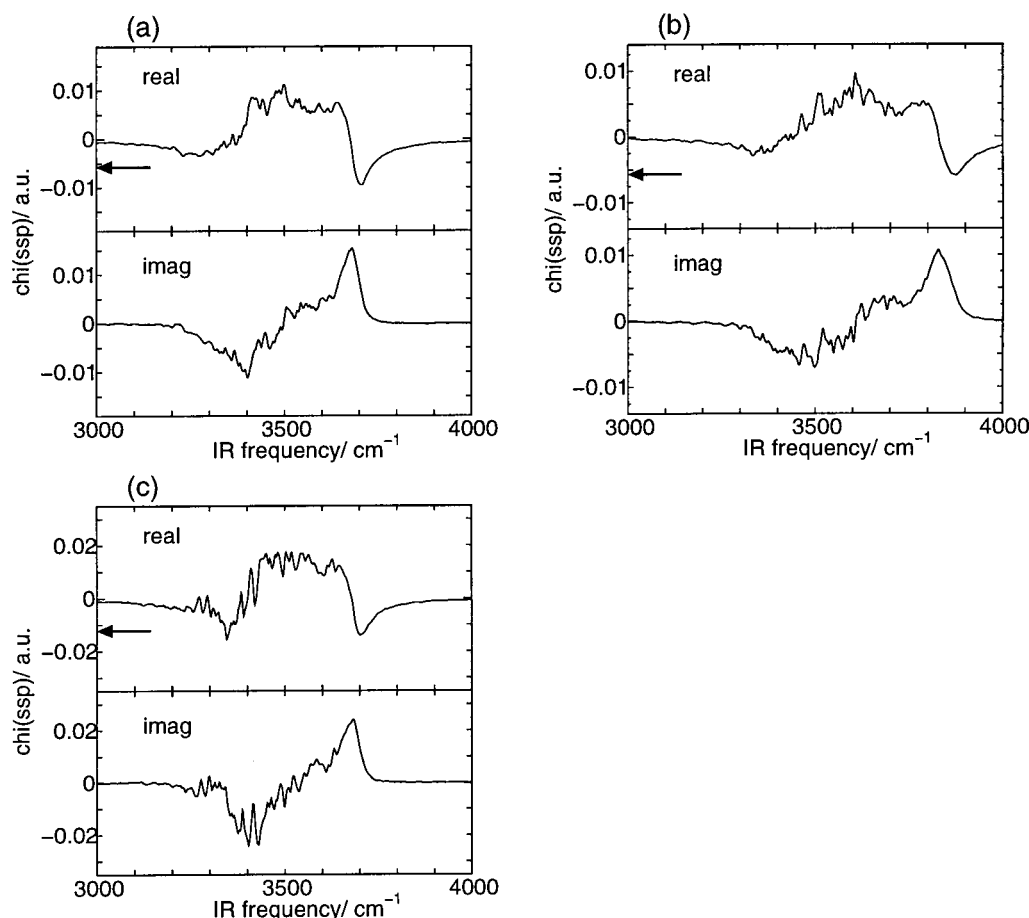
Figure 7. The *XXZ* nonlinear susceptibility of the water surface. Panels a, b, and c correspond to the three models in Figure 6. The upper and lower panels of each case show, respectively, the real and imaginary parts. The solid curves indicate the resonant components calculated via eq 7, and the arrows indicate the nonresonant components calculated via eq 8, assumed to be independent of the IR frequency. Units are cm^{-1} for the abscissas and au for the ordinates.

of the intramo-lecular vibrations and induced electronic polarization. The present formula removes most of the approximations and empirical parameters in our previous treatment, for example, those involving the damping factor, the nonresonant susceptibility, the local field correction, etc, and thus can be considered to be quite rigorous within the classical MD methodology and the dipole approximation of the susceptibility.

The new treatment has been applied to the water surface to examine its performance, and the simulated spectra successfully reproduce qualitative features of the experimental line shape (although we recall that currently there are discrepancies between different experimental results). The effect of the induced electronic polarization on the SFG spectra is less marked than that on the IR spectra but is still significant for the relative intensity of the low-frequency hydrogen-bonded band compared to the high-frequency "dangling bond" one. Overall, the comparison with experiment indicates that while the high-frequency dangling bond region of the spectrum is quite well described, further improvement is required in the low-frequency band assigned to hydrogen-bonded OH vibrations. Among the limited number of factors not included in the present treatment, possibly one of the most significant is the contribution of the induced quadrupole. While the dipolar contribution, examined here, has been suggested to dominate the SFG signal,[56] a quantitative evaluation of the quadrupolar contribution has yet to be made. Because an induced quadrupole is not restricted to the surface because of symmetry considerations, it is possible

that any quadrupolar contribution may have more influence on the signal from the deeper region of the surface. This issue will definitely be pursued in future work because it involves the fundamental question of the surface-sensitive character of an SFG spectrum.

However, even without any further improvements, the present theory itself would at the very least be useful if our focus is on the surface structure of the very top monolayer. This is itself of very considerable interest because the high-frequency peak of the dangling hydrogen bonds is often very sensitive to small perturbations. For example, a small amount of sulfuric acid remarkably suppresses its intensity.[14] We plan to employ the present theory for SFG spectra, as well as subsequent extensions, to the molecular-level characterization of aqueous aerosol surfaces, particularly those of atmospheric importance.

Appendix A. Hyperpolarizability Tensor Expression

The frequency-dependent molecular polarizability, $\alpha_{pq}(\omega)$, and the hyperpolarizability, $\beta_{pqr}(\omega_{SFG}, \omega_{vis}, \omega_{IR})$, are expressed

Theoretical Analysis of SFG Spectrum

J. Phys. Chem. B, Vol. 106, No. 3, 2002 **683**

using the second- and third-order perturbation formalisms. The explicit formulas are[15]

$$\alpha_{pq}(\omega) = \sum_{g,n} \left[-\frac{\langle g|\mu_p|n\rangle\langle n|\mu_q|g\rangle}{\omega - \omega_{ng} + i\gamma_{ng}} + \frac{\langle g|\mu_q|n\rangle\langle n|\mu_p|g\rangle}{\omega + \omega_{ng} + i\gamma_{ng}} \right]\rho_g^{(0)} \quad (35)$$

$$\beta_{pqr}(\omega_{SFG},\omega_{vis},\omega_{IR}) = \sum_{g,n,m}$$

$$\left[\frac{\langle g|\mu_p|n\rangle\langle n|\mu_q|m\rangle\langle m|\mu_r|g\rangle}{(\omega_{SFG} - \omega_{ng} + i\gamma_{ng})(\omega_{IR} - \omega_{mg} + i\gamma_{mg})} + \right.$$

$$\frac{\langle g|\mu_p|n\rangle\langle n|\mu_r|m\rangle\langle m|\mu_q|g\rangle}{(\omega_{SFG} - \omega_{ng} + i\gamma_{ng})(\omega_{vis} - \omega_{mg} + i\gamma_{mg})} +$$

$$\frac{\langle g|\mu_r|m\rangle\langle m|\mu_q|n\rangle\langle n|\mu_p|g\rangle}{(\omega_{SFG} + \omega_{ng} + i\gamma_{ng})(\omega_{IR} + \omega_{mg} + i\gamma_{mg})} +$$

$$\frac{\langle g|\mu_q|m\rangle\langle m|\mu_r|n\rangle\langle n|\mu_p|g\rangle}{(\omega_{SFG} + \omega_{ng} + i\gamma_{ng})(\omega_{vis} + \omega_{mg} + i\gamma_{mg})} -$$

$$\frac{\langle n|\mu_q|g\rangle\langle m|\mu_p|n\rangle\langle g|\mu_r|m\rangle}{(\omega_{SFG} - \omega_{nm} + i\gamma_{nm})} \left(\frac{1}{\omega_{IR} + \omega_{mg} + i\gamma_{mg}} + \right.$$

$$\left. \frac{1}{\omega_{vis} - \omega_{ng} + i\gamma_{ng}} \right) - \frac{\langle n|\mu_r|g\rangle\langle m|\mu_p|n\rangle\langle g|\mu_q|m\rangle}{(\omega_{SFG} - \omega_{nm} + i\gamma_{nm})}$$

$$\left. \left(\frac{1}{\omega_{IR} - \omega_{ng} + i\gamma_{ng}} + \frac{1}{\omega_{vis} + \omega_{mg} + i\gamma_{mg}} \right) \right]\rho_g^{(0)} \quad (36)$$

Here $|g\rangle$ is an initial state with the thermal equilibrium distribution $\rho_g^{(0)}$, and $|n\rangle$ and $|m\rangle$ are the intermediate (electronic + vibrational) states. ω_{ng} and γ_{ng} are the energy gap $E_n - E_g$ and the damping factor between the state $|g\rangle$ and $|n\rangle$ (Note that $\omega_{ng} = -\omega_{gn}$ and $\gamma_{ng} = \gamma_{gn}$). The fifth and sixth terms of eq 36 are given as

$$[\text{fifth term}] = -\frac{\langle n|\mu_q|g\rangle\langle m|\mu_p|n\rangle\langle g|\mu_r|m\rangle}{(\omega_{IR} + \omega_{mg} + i\gamma_{mg})(\omega_{vis} - \omega_{ng} + i\gamma_{ng})}$$

$$\frac{\omega_{SFG} - \omega_{nm} + i(\gamma_{ng} + \gamma_{mg})}{\omega_{SFG} - \omega_{nm} + i\gamma_{nm}} \approx$$

$$-\frac{\langle n|\mu_q|g\rangle\langle m|\mu_p|n\rangle\langle g|\mu_r|m\rangle}{(\omega_{IR} + \omega_{mg} + i\gamma_{mg})(\omega_{vis} - \omega_{ng} + i\gamma_{ng})} \quad (37)$$

$$[\text{sixth term}] = -\frac{\langle n|\mu_r|g\rangle\langle m|\mu_p|n\rangle\langle g|\mu_q|m\rangle}{(\omega_{IR} - \omega_{ng} + i\gamma_{ng})(\omega_{vis} + \omega_{mg} + i\gamma_{mg})}$$

$$\frac{\omega_{SFG} - \omega_{nm} + i(\gamma_{ng} + \gamma_{mg})}{\omega_{SFG} - \omega_{nm} + i\gamma_{nm}} \approx -$$

$$\frac{\langle n|\mu_r|g\rangle\langle m|\mu_p|n\rangle\langle g|\mu_q|m\rangle}{(\omega_{IR} - \omega_{ng} + i\gamma_{ng})(\omega_{vis} + \omega_{mg} + i\gamma_{mg})} \quad (38)$$

Through the use of eqs 37 and 38, β in eq 36 is represented as

$$\beta_{pqr}(\omega_{SFG},\omega_{vis},\omega_{IR}) = \sum_{g,n,m} \left[-\left(-\frac{\langle g|\mu_p|n\rangle\langle n|\mu_q|m\rangle}{\omega_{SFG} - \omega_{ng} + i\gamma_{ng}} + \right.\right.$$

$$\left. \frac{\langle g|\mu_q|n\rangle\langle n|\mu_p|m\rangle}{\omega_{vis} + \omega_{ng} + i\gamma_{ng}} \right) \frac{\langle m|\mu_r|g\rangle}{\omega_{IR} - \omega_{mg} + i\gamma_{mg}} -$$

$$\left(-\frac{\langle g|\mu_p|n\rangle\langle n|\mu_r|m\rangle}{\omega_{SFG} - \omega_{ng} + i\gamma_{ng}} + \right.$$

$$\left. \frac{\langle g|\mu_r|n\rangle\langle n|\mu_p|m\rangle}{\omega_{IR} + \omega_{ng} + i\gamma_{ng}} \right) \frac{\langle m|\mu_q|g\rangle}{\omega_{vis} - \omega_{mg} + i\gamma_{mg}} +$$

$$\left(\frac{\langle g|\mu_q|n\rangle\langle n|\mu_r|m\rangle}{\omega_{vis} + \omega_{ng} + i\gamma_{ng}} + \right.$$

$$\left. \frac{\langle g|\mu_r|n\rangle\langle n|\mu_q|m\rangle}{\omega_{IR} + \omega_{ng} + i\gamma_{ng}} \right) \frac{\langle m|\mu_p|g\rangle}{\omega_{SFG} + \omega_{mg} + i\gamma_{mg}} \right]\rho_g^{(0)} \quad (39)$$

The parenthesis of the first term can be replaced with $\langle g|\alpha_{pq}(\omega_{SFG})|m\rangle$ (or $\langle g|\alpha_{pq}(\omega_{vis})|m\rangle$) using eq 35, assuming $1/(\omega_{SFG} - \omega_{ng} + i\gamma_{ng}) \approx 1/(\omega_{vis} - \omega_{ng} + i\gamma_{ng})$ (or $1/(\omega_{vis} + \omega_{ng} + i\gamma_{ng}) \approx 1/(\omega_{SFG} + \omega_{ng} + i\gamma_{ng})$) in the denominator. These matrix elements are further approximated with the static polarizability, $\langle g|\alpha_{pq}(\omega=0)|m\rangle$, because ω_{SFG} and ω_{vis} are usually far short of the electronic transition energy and totally off-resonant. Thus the first term of eq 39 leads to

$$[\text{first term}] = \sum_{g,m} \left[-\frac{\langle g|\alpha_{pq}|m\rangle\langle m|\mu_r|g\rangle}{\omega_{IR} - \omega_{mg} + i\gamma_{mg}} \right]\rho_g^{(0)} \quad (40)$$

which agrees with the resonant term of the hyperpolarizability, β_{pqr}^R of eq 2, where the summations over g and m are restricted to the vibrational manifolds in the electronic ground state. The restriction on the g states is reasonable under the usual thermal conditions where the occupation of the electronic excited states is negligible, and the restriction on m is justified because the contribution from electronic excited states becomes insignificant because of the very small denominator, $1/(\omega_{IR} - \omega_{mg} + i\gamma_{mg})$ in eq 40.

The remaining two terms in eq 39 correspond to the nonresonant component, β_{pqr}^{NR} in eq 1. These terms could be approximated with the static polarizability in the same way,

$$[\text{second and third terms}] \rightarrow \sum_{g,m} \left[-\frac{\langle g|\alpha_{pr}|m\rangle\langle m|\mu_q|g\rangle}{\omega_{vis} - \omega_{mg} + i\gamma_{mg}} + \right.$$

$$\left. \frac{\langle g|\alpha_{qr}|m\rangle\langle m|\mu_p|g\rangle}{\omega_{SFG} + \omega_{mg} + i\gamma_{mg}} \right]\rho_g^{(0)} \quad (41)$$

but eq 41 should be less useful than eq 40 because (i) the introduction of the polarizability matrix element, $\langle g|\alpha_{pr}|m\rangle$ (or $\langle g|\alpha_{qr}|m\rangle$) in eq 41, is not well-justified and (ii) electronic excited states cannot be neglected in the intermediate states, m, in eq 41. Item i is understood by comparing eq 35 with the second and third terms in the parentheses in eq 39, which are to be replaced with the polarizability matrix elements in eq 41. One notices that significant differences in the denominators have to be neglected through the introduction of the polarizability matrix elements. This means that fairly crude approximations

have to be invoked, assuming $1/(\omega_{IR} + \omega_{ng} + i\gamma_{ng}) \approx 1/(\omega_{SFG} + \omega_{ng} + i\gamma_{ng})$ for the second term and $1/(\omega_{IR} + \omega_{ng} + i\gamma_{ng}) \approx -1/(\omega_{vis} - \omega_{ng} + i\gamma_{ng})$ for the third term, but these approximations are not as good as the similar replacement to derive eq 40 because of the large frequency difference between ω_{IR} and ω_{SFG} (or ω_{vis}). The second item (ii) is attributed to the electronic excitation frequency, ω_{mg}, being possibly close to the visible or SFG frequency, though the electronic excited states could be neglected in eq 40 because of the large energy gap between the excitation frequency and the IR frequency. In fact, we have attempted to evaluate the nonresonant hyperpolarizability via the time-dependent formula derived from the approximate eq 41, but the values thus calculated severely underestimate the nonresonant component, by an order of magnitude. We believe that the main reason for this failure is the lack of evaluated contribution of intermediate excited electronic states m, which are certainly not picked up in the MD time propagation. Accordingly, we abandoned eq 41 and have instead employed eq 5 for the evaluation of the nonresonant term.

Appendix B. Hyperpolarizability Symmetry Number

Here, we derive the symmetry number σ in eq 5. The left-hand side of eq 5 denotes the frequency-dependent hyperpolarizability, while the right-hand side denotes the static one. The frequency-dependent hyperpolarizability, $\beta(\omega_1,\omega_2,\omega_3)$, satisfies the following equation:

$$p_p(\omega_1) = \sum_q \alpha_{pq}(\omega_1)E_q(\omega_1) + \sum_{q,r}\beta_{pqr}(\omega_1,\omega_2,\omega_3)E_q(\omega_2)E_r(\omega_3) + ... \quad (42)$$

where the suffices p, q, and r range over x, y, and z and $p_p(\omega_1)$ is the induced dipole moment at frequency ω_1. On the other hand, the static polarizability and hyperpolarizability are defined as

$$\alpha_{pq}^{static} = \left(\frac{\partial p_p}{\partial E_q}\right)_{E=0}, \quad \beta_{pqr}^{static} = \left(\frac{\partial^2 p_p}{\partial E_q \partial E_r}\right)_{E=0} \quad (43)$$

and hence, the dipole moment in a static electric field is represented as

$$p_p^{static} = (p_p)_{E=0} + \sum_q \alpha_{pq}^{static}E_q + \frac{1}{2}\sum_{q,r}\beta_{pqr}^{static}E_qE_r + ... \quad (44)$$

where $(p_p)_{E=0}$ is the permanent dipole moment. Comparing eqs 42 and 44, one can derive $\sigma = 1/2$ in eq 5. This factor originates from the two indistinguishable electric fields, E_q and E_r, in eq 44, while they are distinguishable in eq 42, having different frequencies.

References and Notes

(1) Eisenthal, K. B. *Chem. Rev.* **1996**, *96,* 1343.
(2) Corn, R. M.; Higgins, D. A. *Chem. Rev.* **1994**, *94,* 107.
(3) Tadjeddine, A.; Peremans, A. *Surf. Sci.* **1996**, *368,* 377.
(4) Somorjai, G. A.; Rupprechter, G. *J. Phys. Chem. B* **1999**, *103,* 1623.
(5) Shen, Y. R. In *Proceedings of the International School of Physics "Enrico Fermi"*; Hansch, T., Inguscio, M., Eds.; North-Holland: Amsterdam, 1994; Vol. 120, p 139.
(6) Shultz, M. J.; Schnitzer, C.; Simonelli, D.; Baldelli, S. *Int. Rev. Phys. Chem.* **2000**, *19,* 123.
(7) Allen, H. C.; Gragson, D. E.; Richmond, G. L. *J. Phys. Chem. B* **1999**, *103,* 660.
(8) Brown, M. G.; Raymond, E. A.; Allen, H. C.; Scatena, L. F.; Richmond, G. L. *J. Phys. Chem. A* **2000**, *104,* 10220.

(9) Allen, H. C.; Raymond, E. A.; Richmond, G. L. *J. Phys. Chem. A* **2001**, *105,* 1649.
(10) Geiger, F. M.; Tridico, A. C.; Hicks, J. M. *J. Phys. Chem. B* **1999**, *103,* 8205.
(11) Donaldson, D. J.; Guest, J. A.; Goh, M. C. *J. Phys. Chem.* **1995**, *99,* 9313.
(12) Schnitzer, C.; Baldelli, S.; Shultz, M. J. *Chem. Phys. Lett.* **1999**, *313,* 416.
(13) Baldelli, S.; Schnitzer, C.; Shultz, M. J.; Campbell, D. J. *J. Phys. Chem. B* **1997**, *101,* 10435.
(14) Radüge, C.; Pflumio, V.; Shen, Y. R. *Chem. Phys. Lett.* **1997**, *274,* 140.
(15) Shen, Y. R. *Principle of Nonlinear Optics*; Wiley: New York, 1984.
(16) Dick, B. *Chem. Phys.* **1985**, *96,* 199.
(17) Superfine, R.; Huang, J. Y.; Shen, Y. R. *Phys. Rev. Lett.* **1991**, *66,* 1066.
(18) Hirose, C.; Yamamoto, H.; Akamatsu, N.; Domen, K. *J. Phys. Chem.* **1993**, *97,* 10064.
(19) Zhang, D.; Gutow, J.; Eisenthal, K. B. *J. Phys. Chem.* **1994**, *98,* 13729.
(20) Morita, A.; Hynes, J. T. *Chem. Phys.* **2000**, *258,* 371.
(21) Yeh, Y. L.; Zhang, C.; Held, H.; Mebel, A. M.; Wei, X.; Lin, S. H.; Shen, Y. R. *J. Chem. Phys.* **2001**, *114,* 1837.
(22) See, for example: Bianco, R.; Hynes, J. T. In *Theoretical Methods in Condensed Phase Chemistry*; Schwartz, S. D., Ed.; Kluwer: Dordrecht, Netherlands, 2000 and references therein.
(23) Pouthier, V.; Hoang, P. N. M.; Girardet, C. *J. Chem. Phys.* **1999**, *110,* 6963.
(24) McQuarrie, D. A. *Statistical Mechanics*; University Science Books: Herndon, VA, 2000.
(25) Wei, X.; Shen, Y. R. *Phys. Rev. Lett.* **2001**, *86,* 4799.
(26) Huggins, C. M.; Pimentel, G. C. *J. Phys. Chem.* **1956**, *60,* 1615.
(27) Pimentel, G. C.; McClellan, A. L. *The Hydrogen Bond*; W. H. Freeman: San Francisco, 1960; Chapter 3.
(28) Zilles, B. A.; Person, W. B. *J. Chem. Phys.* **1983**, *79,* 65.
(29) Thompson, W. H.; Hynes, J. T. *J. Am. Chem. Soc.* **2000**, *122,* 6278 and references therein.
(30) The valence bond mode of analysis of charge transfer in hydrogen bonds employed in ref 29 cannot be extended to the water system examined here; this could possibly be examined in future work in a Car−Parinello approach. (a) Car, R.; Parrinello, M. *Phys. Rev. Lett.* **1985**, *55,* 2471. (b) Laasonen, K.; Sprik, M.; Parrinello, M.; Car, R. *J. Chem. Phys.* **1993**, *99,* 9080.
(31) Fröhlich, H. *Theory of Dielectrics*; Clarendon: Oxford, U.K., 1958.
(32) Becke, A. D. *J. Chem. Phys.* **1993**, *98,* 5648.
(33) Lee, C.; Yang, W.; Parr, R. G. *Phys. Rev.* **1988**, *B37,* 785.
(34) Frisch, M. J.; Trucks, G. W.; Schlegel, H. B.; Scuseria, G. E.; Robb, M. A.; Cheeseman, J. R.; Zakrzewski, V. G.; Montgomery, J. A., Jr.; Stratmann, R. E.; Burant, J. C.; Dapprich, S.; Millam, J. M.; Daniels, A. D.; Kudin, K. N.; Strain, M. C.; Farkas, O.; Tomasi, J.; Barone, V.; Cossi, M.; Cammi, R.; Mennucci, B.; Pomelli, C.; Adamo, C.; Clifford, S.; Ochterski, J.; Petersson, G. A.; Ayala, P. Y.; Cui, Q.; Morokuma, K.; Malick, D. K.; Rabuck, A. D.; Raghavachari, K.; Foresman, J. B.; Cioslowski, J.; Ortiz, J. V.; Stefanov, B. B.; Liu, G.; Liashenko, A.; Piskorz, P.; Komaromi, I.; Gomperts, R.; Martin, R. L.; Fox, D. J.; Keith, T.; Al-Laham, M. A.; Peng, C. Y.; Nanayakkara, A.; Gonzalez, C.; Challacombe, M.; Gill, P. M. W.; Johnson, B. G.; Chen, W.; Wong, M. W.; Andres, J. L.; Head-Gordon, M.; Replogle, E. S.; Pople, J. A. *Gaussian 98*, revision A.6; Gaussian, Inc.: Pittsburgh, PA, 1998.
(35) Woon, D. E.; Dunning, T. H., Jr. *J. Chem. Phys.* **1994**, *100,* 2975.
(36) Morita, A.; Kato, S. *J. Chem. Phys.* **1999**, *110,* 11987.
(37) Oki, M. et al., Eds. *Kagaku Binran*, 4th ed.; Maruzen: Tokyo, 1993 (in Japanese).
(38) $9 \times (8 \times 9/2) = 324$, taking account of the two equivalent hydrogens.
(39) Ferguson, D. M. *J. Comput. Chem.* **1995**, *15,* 501.
(40) Berendsen, H. J. C.; Postma, J. P. M.; van Gunsteren, M. F.; Hermans, J. In *Intermolecular Forces*; Pullman, B., Ed.; Reidel: Dordrecht, Netherlands, 1981.
(41) Chen, S. H.; Toukan, K.; Loong, C. K.; Price, D. L.; Teixeira, J. *Phys. Rev. Lett.* **1984**, *53,* 1360.
(42) Kuchitsu, K.; Morino, Y. *Bull. Chem. Soc. Jpn.* **1965**, *38,* 814.
(43) Ahlborn, H.; Ji, X.; Space, B.; Moore, P. B. *J. Chem. Phys.* **1999**, *111,* 10622.
(44) Allen, M. P.; Tildesley, D. J. *Computer Simulation of Liquids*; Oxford University Press: New York, 1991.
(45) In our previous paper,[20] the long-range correction based on the continuum model was employed.[46,47] However, this correction was fairly time-consuming, making the overall CPU time 6 times as much. While the long-range correction affects certain thermodynamic properties such as surface tension, it does not significantly affect the local structure of surface,[48] which is our main focus here.
(46) Torrie, G. M.; Valleau, J. P. *J. Chem. Phys.* **1980**, *73,* 5807.

Theoretical Analysis of SFG Spectrum

J. Phys. Chem. B, Vol. 106, No. 3, 2002 **685**

(47) Valleau, J. P.; Gardner, A. A. *J. Chem. Phys.* **1987**, *86,* 4162.

(48) Taylor, R. S.; Dang, L. X.; Garrett, B. C. *J. Phys. Chem.* **1996**, *100,* 11720.

(49) Matsumoto, M.; Kataoka, Y. *J. Chem. Phys.* **1988**, *88,* 3233.

(50) Berendsen, H. J. C.; Grigera, J. R.; Straatsma, T. P. *J. Phys. Chem.* **1987**, *91,* 6269.

(51) The surface thickness is known to be sensitive to the force field employed and the correction of the long-range interaction. Sokhan, V. P.; Tildesley, D. J. *Mol. Phys.* **1997**, *92, 625.*

(52) Downing, H. D.; Williams, D. *J. Geophys. Res.* **1975**, *80,* 1656.

(53) Walrafen, G. E. *J. Chem. Phys.* **1967**, *47,* 114.

(54) Bertie, J. E.; Lan, Z. *Appl. Spectrosc.* **1996**, *50,* 1047.

(55) Benjamin, I. *Phys. Rev. Lett.* **1994**, *73,* 2083.

(56) Du, Q.; Superfine, R.; Freysz, E.; Shen, Y. R. *Phys. Rev. Lett.* **1993**, *70,* 2313.

(57) Schnizer, C.; Baldelli, S.; Campbell, D. J.; Shultz, M. J. *J. Phys. Chem. A* **1999**, *103,* 6383.

(58) The experiments in Figure 5 were performed at different temperatures: (a) 40 °C;[56] (b) 5 °C;[57] (c) 20 °C.[9] However, the difference in temperature is not likely the reason for the different spectral shapes; ref 56 discussed the temperature dependence, concluding that there is no significant change over 10−80 °C in the water SFG spectra.